

NJC

Accepted Manuscript



This is an *Accepted Manuscript*, which has been through the Royal Society of Chemistry peer review process and has been accepted for publication.

Accepted Manuscripts are published online shortly after acceptance, before technical editing, formatting and proof reading. Using this free service, authors can make their results available to the community, in citable form, before we publish the edited article. We will replace this *Accepted Manuscript* with the edited and formatted *Advance Article* as soon as it is available.

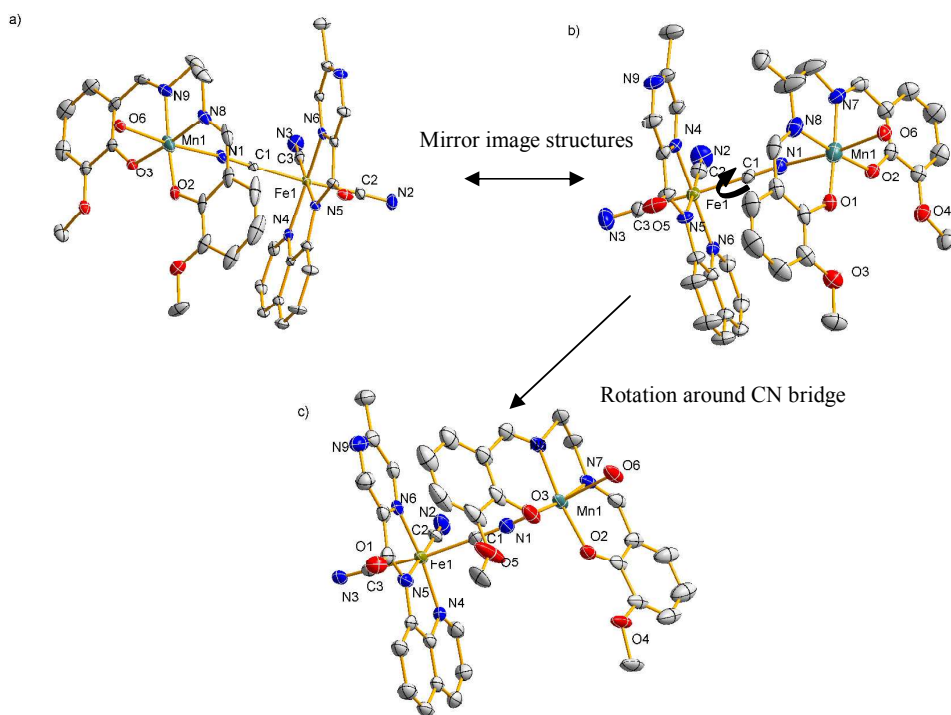
You can find more information about *Accepted Manuscripts* in the [Information for Authors](#).

Please note that technical editing may introduce minor changes to the text and/or graphics, which may alter content. The journal's standard [Terms & Conditions](#) and the [Ethical guidelines](#) still apply. In no event shall the Royal Society of Chemistry be held responsible for any errors or omissions in this *Accepted Manuscript* or any consequences arising from the use of any information it contains.

Crystal Structures and Magneto-Structural Correlation Analysis for Several Cyano-Bridged Bimetallic Complexes Based on Mn^{III}-Fe^{III} Systems

Hongbo Zhou,^a Yingying Wang,^a Fangyou Mou,^a Xiaoping Shen,^{*a} and Yashu Liu^b

The rotation of subunits and its influence on magnetic coupling in Mn^{III}-Fe^{III} systems



Cite this: DOI: 10.1039/c0xx00000x

www.rsc.org/xxxxxx

ARTICLE TYPE

Crystal Structures and Magneto-Structural Correlation Analysis for Several Cyano-Bridged Bimetallic Complexes Based on Mn^{III}-Fe^{III} Systems

Hongbo Zhou,^a Yingying Wang,^a Fangyou Mou,^a Xiaoping Shen,^{*a} and Yashu Liu^b

⁵ Received (in XXX, XXX) Xth XXXXXXXXXX 20XX, Accepted Xth XXXXXXXXXX 20XX

DOI: 10.1039/b000000x

Six new cyano-bridged dinuclear Mn^{III}-NC-Fe^{III} complexes, [Mn^{III}(3-CH₃O-salen)(H₂O)][Fe^{III}(mpzqc)(CN)₃]·CH₃CN·H₂O (**1**), [Mn^{III}(3-CH₃O-salpn)(H₂O)][Fe^{III}(mpzqc)(CN)₃] (**2**), [Mn^{III}(3-CH₃O-salen)(H₂O)][Fe^{III}(mpzqc)(CN)₃] (**3**), [Mn^{III}(3,5-(t-Bu)₂-salen)(CH₃OH)][Fe^{III}(qcq)(CN)₃]·CH₃OH·CH₃CN·2H₂O (**4**), [Mn^{III}(3,5-(t-Bu)₂-salpn)(H₂O)][Fe^{III}(qcq)(CN)₃]·3H₂O (**5**), [Mn^{III}(3-CH₃CH₂O-salpn)(H₂O)][Fe^{III}(qcq)(CN)₃]·CH₃OH·2CH₃CN (**6**) (salen = *N,N'*-ethylenebis(salicylideneiminato) dianion; salpn = *N,N'*-1,2-propylenebis(salicylideneiminato)dianion) derived from Mn^{III}(Schiff base) and *mer*-[Fe^{III}(L)(CN)₃]⁻ (L = mpzqc, qcq; mqzqc = 8-(5-methylpyrazine-2-carboxamido)quinoline; qcq = 8-(2-quinoline-2-carboxamido)quinoline) have been synthesized, structurally characterized and magnetically studied. The X-ray single crystal diffraction analysis indicates that all of these complexes are cyano-bridged Mn^{III}-NC-Fe^{III} dinuclear structures. However, they show variable molecular geometric parameters and structures. Interestingly, the structural subunits of Mn^{III}(Schiff base) and [Fe^{III}(L)(CN)₃]⁻ can rotate around the cyanide bridges. Magnetic investigation indicates that the intramolecular magnetic coupling is dependent on the critical geometric parameters, leading to ferromagnetic nature for **1-3** and **6** but antiferromagnetic for **4** and **5**. Furthermore, the field induced metamagnetic properties detected for **1-3** and **6** are well clarified from analysis of the magneto-structural correlation.

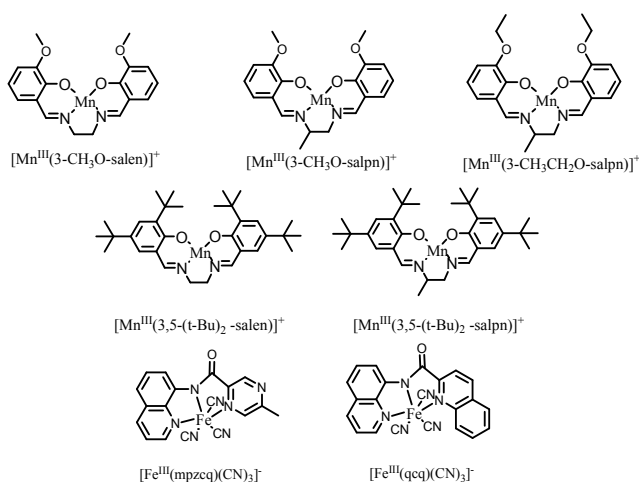
Introduction

In the recent two decades, the research of molecule-based magnets have evolved from traditional 3-D magnets to recent low dimensional magnets because of their interesting magnetic properties and potential applications in molecular devices, high-density information storage and quantum computers, *etc.*¹⁻¹⁰ For designing 3-D magnets, the hexacyanometalates are useful building blocks and they have contributed to a series of 3-D magnets with the Curie temperature as high as room temperature.¹¹⁻¹⁴ However, for the formation of the low-dimensional systems, the chelating ligands need be introduced into these building blocks to limit the oligomerization or polymerization effect. As a result, these hexacyanometalates have been replaced by the so-called modified hexacyanometalates [(L)M(CN)₆]^{q-} (M = Fe, Cr; *etc.* L = blocking group) to explore new low dimensional systems. Based on this strategy, a large number of low dimensional complexes featuring interesting structures and magnetism have been reported.¹⁵⁻⁴³

In our group, we have been focusing on investigating the magnetic systems based on Mn^{III}(Schiff base) and the cyanometalates building blocks such as [M(CN)₆]³⁻, [(L)M(CN)₄]⁻, [(L)M(CN)₃]²⁻ and [(L)M(CN)₂]³⁻ (M = Fe, Cr; *etc.*).

⁴⁵ The selection of Mn^{III}(Schiff base) is due to the large spin value (*S*_T) and strong magnetic anisotropy of Mn^{III} ions, which are stabilized by the Schiff base ligands. The introduction of functional groups on the Schiff base ligands facilitates tuning the ligand field around Mn^{III} ion and further influence the versatility for reactivity and availability of structures. Furthermore, the functional groups on the Schiff base ligands also play an important role in determining the intermolecular short contacts and thus affect the final magnetic properties. For the cyanometalates building blocks, *fac*-tricyanidoferrates [Fe^{III}(L)(CN)₃]⁻ are thoroughly investigated.⁴⁴⁻⁵⁰ Recently, *mer*-tricyanidoferrate building blocks such as [Fe^{III}(bpca)(CN)₃]⁻,^{51,52} [Fe^{III}(pcq)(CN)₃]⁻,⁵³ [Fe^{III}(pzqc)(CN)₃]⁻,⁵⁴ [Fe^{III}(mpzqc)(CN)₃]⁻,⁵⁵ [Fe^{III}(qcq)(CN)₃]⁻⁵⁶ were designed and employed to construct new low dimensional complexes. In these relevant complexes, cyano-bridged Mn^{III}-NC-Fe^{III} complexes derived from Mn^{III}(Schiff base) and *mer*-tricyanidoferrate [Fe^{III}(L)(CN)₃]⁻ were often of great interest because of their colorful structural fashions and the interesting magnetic properties.^{20,40,45,53,55,56} To our knowledge, the assembly of [Mn^{III}(Schiff base)]⁺ cation and *mer*-[Fe^{III}(L)(CN)₃]⁻ anion often induces the formation of dinuclear entities (Mn^{III}-NC-Fe^{III})^{45,53,55,56} or zigzag chain structures [(Mn^{III}-NC-Fe^{III})_n].^{39,56} Recently, novel 1-D linear chain⁵³ and branch chain⁴⁰ of (Mn^{III}-NC-Fe^{III})_n were also reported. However,

the magnetic interaction of Mn^{III}-NC-Fe^{III} exchange coupling could be found as ferromagnetic^{15,21,53,57,58} or antiferromagnetic,^{20,53,55,57,58} and the coupling mechanism is still not very clear. Such a difficulty in understanding the magnetism might be due to subtle convolution of geometrical parameters such as bond lengths, bond angles and bond torsion angles in these systems. In this work, six new cyano-bridged dinuclear Mn^{III}-NC-Fe^{III} complexes, [Mn^{III}(3-CH₃O-salen)(H₂O)][Fe^{III}(mpzqc)(CN)₃]·CH₃CN·H₂O (1), [Mn^{III}(3-CH₃O-salpn)(H₂O)][Fe^{III}(mpzqc)(CN)₃] (2), [Mn^{III}(3-CH₃O-salen)(H₂O)][Fe^{III}(mpzqc)(CN)₃] (3), [Mn^{III}(3,5-(t-Bu)₂-salen)(CH₃OH)][Fe^{III}(qcq)(CN)₃]·CH₃OH·CH₃CN·2H₂O (4), [Mn^{III}(3,5-(t-Bu)₂-salpn)(H₂O)][Fe^{III}(qcq)(CN)₃]·3H₂O (5), [Mn^{III}(3-CH₃CH₂O-salpn)(H₂O)][Fe^{III}(qcq)(CN)₃]·CH₃OH·2CH₃CN (6) (salen = N,N'-ethylenebis(salicylideneiminato) dianion; salpn = N,N'-1,2-propylenebis(salicylideneiminato)dianion) derived from Mn^{III}(Schiff base) and mer-[Fe^{III}(L)(CN)₃]⁻ (Scheme 1) (L = mpzqc, qcq; mqzqc = 8-(5-methylpyrazine-2-carboxamido)quinoline; qcq = 8-(2-quinoline-2-carboxamido)quinoline) were synthesized. Notably, these complexes show a continuous change of molecular geometric parameters, which provide a unique opportunity to understand the complicated magneto-structural correlation of these low dimensional systems.



Scheme 1 [Mn^{III}(Schiff-base)]⁺ cations and [Fe^{III}(L)(CN)₃]⁻ anions used in this work.

Experimental

Materials

All chemicals and solvents in the synthesis were of reagent grade and used as received without further purification. The starting materials of K[Fe^{III}(mqzqc)(CN)₃]·H₂O, PPh₄[Fe^{III}(mqzqc)(CN)₃]·H₂O,⁵⁵ K[Fe^{III}(qcq)(CN)₃]·H₂O, PPh₄[Fe^{III}(qcq)(CN)₃]·H₂O,⁵⁶ [Mn^{III}(3-CH₃O-salen)(H₂O)]ClO₄, [Mn^{III}(3-CH₃O-salpn)(H₂O)]ClO₄, [Mn^{III}(3,5-(t-Bu)₂-salen)(H₂O)]ClO₄, [Mn^{III}(3,5-(t-Bu)₂-salpn)(H₂O)]ClO₄ and

[Mn^{III}(3-CH₃CH₂O-salpn)(H₂O)]ClO₄⁵⁹ were prepared as described in the literatures.

Caution! Cyanides are very toxic and perchlorate salts are potentially explosive. Although no problems were experienced during our experiments, it is highly suggested to handling them carefully with small quantities for the safety consideration.

Preparations

[Mn^{III}(3-CH₃O-salen)(H₂O)][Fe^{III}(mpzqc)(CN)₃]·CH₃CN·H₂O (1). An acetonitrile solution (10 mL) of [Mn^{III}(3-CH₃O-salen)(H₂O)]ClO₄ (0.05 mmol) was slowly added to an aqueous solution (10 mL) of K[Fe^{III}(mqzqc)(CN)₃]·H₂O (0.05 mmol). Slow evaporation of the resulting solution in dark at room temperature yielded black rod crystals of complex 1 in two weeks, which were washed with acetonitrile and water, respectively, and dried in air. Anal. found: C, 53.20; H, 4.35; N, 16.50%. Calcd for C₃₈H₃₆FeMnN₁₀O₇: C, 53.35; H, 4.24; N, 16.37%. IR: ν_{max}/cm⁻¹ 3418(s), 2121(m), 1625(s), 1542(m), 1504(w), 1462(w), 1436(m), 1381(m), 1342(m), 1282(s), 1221(m), 805(w), 724(m).

[Mn^{III}(3-CH₃O-salpn)(H₂O)][Fe^{III}(mpzqc)(CN)₃] (2). A methanol solution (10 mL) of PPh₄[Fe^{III}(mpzqc)(CN)₃]·H₂O (0.05 mmol) was slowly added to an acetonitrile solution (10 mL) of [Mn^{III}(3-CH₃O-salpn)(H₂O)]ClO₄ (0.05 mmol), then an aqueous solution (10 mL) of Pr(NO₃)₃·6H₂O (0.05 mmol) was added into the mixture. Slow evaporation of the resulting solution in dark at room temperature yielded black rod crystals of complex 2 in two weeks, which were washed with methanol/acetonitrile and water, respectively, and dried in air. Anal. found: C, 54.73; H, 4.25; N, 15.35%. Calcd for C₃₇H₃₃FeMnN₉O₆: C, 54.83; H, 4.10; N, 15.55%. IR: ν_{max}/cm⁻¹ 3420(s), 2119(m), 1620(s), 1542(m), 1504(w), 1462(m), 1436(m), 1382(m), 1342(m), 1284(s), 1221(m), 804(w), 724(m).

[Mn^{III}(3-CH₃O-salen)(H₂O)][Fe^{III}(mpzqc)(CN)₃] (3). Using the same synthetic procedure as complex 2, complex 3 was obtained as black rod crystals by replacing [Mn^{III}(3-CH₃O-salpn)(H₂O)]ClO₄ with [Mn^{III}(3-CH₃O-salen)(H₂O)]ClO₄. Anal. found: C, 54.12; H, 4.05; N, 15.50%. Calcd for C₃₆H₃₁FeMnN₉O₆: C, 54.29; H, 3.92; N, 15.83%. IR: ν_{max}/cm⁻¹ 3420(s), 2120(m), 1624(s), 1542(m), 1504(w), 1461(m), 1436(m), 1381(m), 1342(m), 1281(s), 1220(m), 805(w), 724(m).

[Mn^{III}(3,5-(t-Bu)₂-salen)(CH₃OH)][Fe^{III}(qcq)(CN)₃]·CH₃OH·CH₃CN·2H₂O (4). A methanol solution (10 mL) of PPh₄[Fe^{III}(qcq)(CN)₃]·H₂O (0.1 mmol) was slowly added to an acetonitrile solution (10 mL) of [Mn^{III}(3,5-(t-Bu)₂-salen)(H₂O)]ClO₄. Then, one drop of triethylamine was added into the mixture. Slow evaporation of the resulting solution in dark at room temperature yielded black block crystals of complex 4 in two weeks, which were washed with methanol and acetonitrile, respectively, and dried in air. Anal. found: C, 62.35; H, 6.45; N, 11.35%. Calcd for C₅₈H₇₃FeMnN₉O₇: C, 62.25; H, 6.58; N, 11.27%. IR: ν_{max}/cm⁻¹

Table 1 Details of the crystal data and structural refinement parameters of 1–6.

	1	2	3	4	5	6
Formula	C ₃₈ H ₃₆ FeMnN ₁₀ O ₇	C ₃₇ H ₃₃ FeMnN ₉ O ₆	C ₃₆ H ₃₁ FeMnN ₉ O ₆	C ₅₈ H ₇₃ FeMnN ₉ O ₇	C ₅₅ H ₆₈ FeMnN ₈ O ₇	C ₄₈ H ₄₈ FeMnN ₁₀ O ₇
<i>M</i> /g mol ⁻¹	855.5	810.5	796.5	1119.0	1064.0	987.7
Crystal system	monoclinic	monoclinic	triclinic	monoclinic	monoclinic	monoclinic
Space group	<i>P</i> 2 ₁ / <i>n</i>	<i>P</i> 2 ₁ / <i>n</i>	<i>P</i> -1	<i>P</i> 2 ₁ / <i>n</i>	<i>P</i> 2 ₁ / <i>n</i>	<i>P</i> 2 ₁ / <i>n</i>
<i>a</i> /Å	11.933(3)	11.985(3)	11.415(5)	23.328(5)	22.680(5)	13.148(3)
<i>b</i> /Å	14.282(3)	14.249(4)	13.273(5)	10.078(2)	10.109(2)	14.128(3)
<i>c</i> /Å	22.324(4)	22.419(6)	14.081(6)	26.115(5)	26.260(5)	25.240(5)
<i>α</i> /°	90	90	65.735(4)	90.00	90.00	90.00
<i>β</i> /°	94.29(5)	95.528(4)	67.531(4)	100.04(3)	99.76(3)	102.46(3)
<i>γ</i> /°	90	90	71.710(5)	90.00	90.00	90.00
<i>V</i> /Å ³	3794.2(12)	3810.7(17)	1765.9(13)	6045(2)	5933(2)	4578.1(16)
<i>Z</i>	4	4	2	4	4	4
<i>d</i> _{calc} /g cm ⁻³	1.480	1.413	1.498	1.230	1.178	1.404
<i>F</i> (000)	1738.9	1668	818	2364	2206	2009.7
Collected reflections	25133	29140	9765	27526	25493	20028
Observed reflections	6636	7447	5796	11571	10359	8012
Independent reflections	4998	4623	4125	9472	7501	6677
<i>R</i> _{int}	0.0435	0.0732	0.0277	0.0482	0.0810	0.0527
data/restraints/parameters	6636/2/504	7447/1/518	5796/0/501	11571/0/700	10359/0/671	8012/0/599
GOF ^c on <i>F</i> ²	1.077	0.978	0.0993	1.092	1.015	1.028
<i>R</i> ₁ ^a (<i>I</i> > 2 <i>σ</i> (<i>I</i>))	0.0684	0.0516	0.0678	0.0594	0.1310	0.0747
<i>wR</i> ₂ ^b (all data)	0.1680	0.1271	0.1639	0.1696	0.2680	0.1671

^a*R*₁ = $\sum ||F_o| - |F_c|| / \sum |F_o|$. ^b*wR*₂ = $[\sum w(F_o^2 - F_c^2)^2 / \sum w(F_o^2)^2]^{1/2}$; *w* = $1/\sigma^2(|F_o|)$. ^cGoodness of fit: GOF = $[\sum w(F_o^2 - F_c^2)^2 / (n - p)]^{1/2}$, where *n* is the number of reflections and *p* is the number of parameters

5

Table 2 Selected bond lengths [Å] and angles [deg°] for 1-6.

	1	2	3
C1-Fe1	1.934(5)	C1-Fe1	1.948(4)
C2-Fe1	1.955(5)	C2-Fe1	1.952(4)
C3-Fe1	1.949(6)	C3-Fe1	1.954(4)
Fe1-N5	1.872(5)	Fe1-N5	1.880(3)
Fe1-N6	1.960(4)	Fe1-N4	1.955(2)
Fe1-N4	1.976(4)	Fe1-N6	1.973(2)
Mn1-O2	1.872(4)	Mn1-O2	1.874(2)
Mn1-O3	1.881(4)	Mn1-O1	1.883(2)
Mn1-N9	1.964(6)	Mn1-N7	1.978(3)
Mn1-N8	1.983(6)	Mn1-N8	1.990(3)
Mn1-O6	2.242(4)	Mn1-N1	2.264(3)
Mn1-N1	2.270(5)	Mn1-O6	2.252(2)
N1-C1-Fe1	176.3(5)	N1-C1-Fe1	176.9(3)
N2-C2-Fe1	177.1(6)	N2-C2-Fe1	178.1(4)
N3-C3-Fe1	178.8(5)	N3-C3-Fe1	176.3(4)
C1-N1-Mn1	159.3(5)	C1-N1-Mn1	157.0(3)
	4	5	6
C1-Fe1	1.938(3)	C1-Fe1	1.952(9)
C2-Fe1	1.953(3)	C2-Fe1	1.928(9)
C3-Fe1	1.957(3)	C3-Fe1	1.946(9)
Fe1-N5	1.884(3)	Fe1-N5	1.890(7)
Fe1-N6	1.986(3)	Fe1-N6	1.979(7)
Fe1-N4	2.016(3)	Fe1-N4	2.019(7)
Mn1-O3	1.867(2)	Mn1-O2	1.854(5)
Mn1-O2	1.871(2)	Mn1-O3	1.858(5)
Mn1-N7	1.981(2)	Mn1-N7	1.984(6)
Mn1-N8	1.990(2)	Mn1-N8	1.984(6)
Mn1-O4	2.277(6)	Mn1-N1	2.242(7)
Mn1-N1	2.263(3)	Mn1-O4	2.340(7)
N1-C1-Fe1	175.3(3)	N1-C1-Fe1	176.7(7)
N2-C2-Fe1	178.9(3)	N2-C2-Fe1	178.7(9)
N3-C3-Fe1	178.7(3)	N2-C3-Fe1	179.2(9)
C1-N1-Mn1	149.0(2)	C1-N1-Mn1	152.7(6)
C1-Fe1		C1-Fe1	1.944(5)
C2-Fe1		C2-Fe1	1.944(5)
C3-Fe1		C3-Fe1	1.956(5)
Fe1-N5		Fe1-N5	1.882(4)
Fe1-N6		Fe1-N4	1.985(4)
Fe1-N4		Fe1-N6	2.027(4)
Mn1-O3		Mn1-O2	1.876(3)
Mn1-O2		Mn1-O3	1.881(3)
Mn1-N7		Mn1-N8	1.966(5)
Mn1-N8		Mn1-N7	1.976(5)
Mn1-O4		Mn1-N1	2.268(4)
Mn1-N1		Mn1-O4	2.281(3)
N1-C1-Fe1		N1-C1-Fe1	175.3(4)
N2-C2-Fe1		N2-C2-Fe1	178.3(4)
N3-C3-Fe1		N3-C3-Fe1	175.4(5)
C1-N1-Mn1		C1-N1-Mn1	165.2(4)

3422(s), 2121(m), 1626(s), 1542(m), 1503(w), 1460(m), 1436(m), 1382(m), 1342(m), 1281(s), 1220(m), 802(w), 720(m).

[Mn^{III}(3,5-(t-Bu)₂-salpn)(H₂O)][Fe^{III}(qcq)(CN)₃]·3H₂O (5).

Using the same synthetic procedure as complex 4, complex 5 was obtained as black block crystals by replacing [Mn^{III}(3,5-(t-Bu)₂-salen)(H₂O)]ClO₄ with [Mn^{III}(3,5-(t-Bu)₂-salpn)(H₂O)]ClO₄. Anal. found: C, 62.12; H, 6.32; N, 11.05%. Calcd for C₅₅H₆₈FeMnN₈O₇: C, 62.09; H, 6.44; N, 10.53%. IR: $\nu_{\max}/\text{cm}^{-1}$ 3424(s), 2121(m), 1625(s), 1542(m), 1503(w), 1462(m), 1438(m), 1382(m), 1342(m), 1280(s), 1220(m), 802(w), 722(m).

[Mn^{III}(3-CH₃CH₂O-salpn)(H₂O)][Fe^{III}(qcq)(CN)₃]·CH₃OH·2CH₃CN (6).

A methanol solution (10 mL) of PPh₄[Fe^{III}(qcq)(CN)₃]·H₂O (0.1 mmol) was slowly added to an acetonitrile solution (10 mL) of [Mn^{III}(3-CH₃CH₂O-salpn)(H₂O)]ClO₄ (0.1 mmol). Then, one drop of triethylamine was added into the mixture. Slow evaporation of the resulting solution in dark at room temperature yielded black block crystals of complex 6 in two weeks, which were washed with methanol and acetonitrile, respectively, and dried in air. Anal. found: C, 58.36; H, 4.85; N, 14.30%. Calcd for C₄₈H₄₈FeMnN₁₀O₇: C, 58.37; H, 4.90; N, 14.18%. IR: $\nu_{\max}/\text{cm}^{-1}$ 3418(s), 2122(m), 1629(s), 1542(m), 1504(w), 1462(m), 1436(m), 1382(m), 1344(m), 1283(s), 1222(m), 806(w), 722(m).

Physical measurements

Elemental analyses for C, H and N were carried out with a Perkin-Elmer 240C analyzer. Infrared (IR) spectra on KBr pellets were measured on a Nicolet FT-170SX spectrometer in the region from 4000 to 400 cm⁻¹. Magnetic data of the microcrystalline samples were recorded on a Quantum Design SQUID magnetometer (MPMP-XL7). Direct current (dc) magnetic susceptibilities were measured in the temperature range of 1.8 - 300 K using an applied magnetic field of 2 kOe. The field dependences of the magnetization were measured at 1.8 K in an applied field up to 70 kOe. Susceptibilities were corrected considering sample holder as the background and the diamagnetic contribution estimated from Pascal constants.⁶⁰

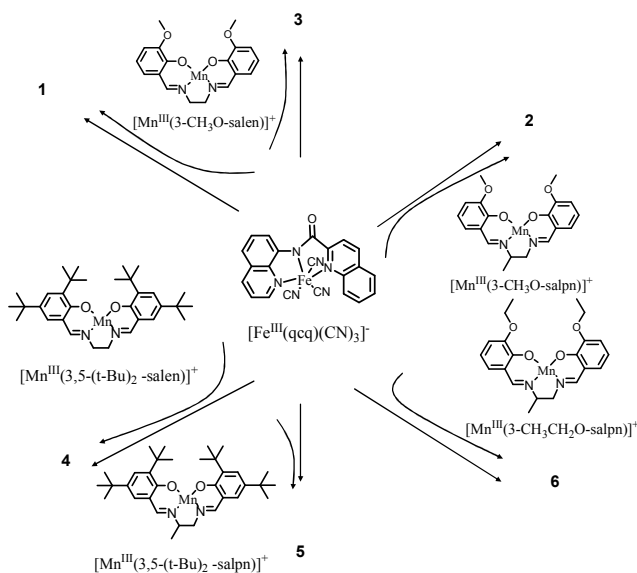
X-Ray crystallography

The diffraction data collection were made at 173 K on a Bruker SMART APEX CCD area detector diffractometer equipped with graphite-monochromated Mo-K_α radiation ($\lambda = 0.71073 \text{ \AA}$). Diffraction data analysis and reduction were performed with SMART, SAINT and XPREP.⁶¹ All the structures were solved by direct methods and refined by a full-matrix least-squares method based on F^2 using the SHELXL crystallographic software package.⁶² All the non-hydrogen atoms were refined anisotropically except for C39, C40, N10 in complex 1, O4, C55 in 4 and C32, C33, C34, C48, O7 in complex 6. These atoms are refined isotropically because of the disorder of them. All hydrogen atoms (except those of the water-H atoms) were included in calculated positions and refined with isotropic thermal parameters derived from the parent atoms. H atoms found on water molecules were located from the residual peaks and included in the refinement with isotropic thermal parameters derived from the water-O atoms. The water-H atoms of O4-O7 in 5 were not found. For complexes 2 and 6, the group of 1, 2-

diaminocyclohexane is slightly disordered and split into two sites. Besides, the atoms of O5, C36 in 3, O4, C55 in 4 are also disordered and split into two sites. For complexes 1, 5 and 6, the non-integer number of atoms in the unit cell is the result of free variable refinement with partial occupancy for some highly disordered solvent molecules. However, these missing atoms (further confirmed by elemental analyses and magnetic measurements) are included in the structural formulas and so there are slightly differences between the reported formulas and the calculated ones. It should be mentioned that the crystal quality of 3 and 5 is not very satisfactory though the data was collected again and again at low temperature. The relatively poor crystal quality should be responsible for the low completeness for 3 and large R value for 5. Also because of this reason, no solvent molecules could be detected in solvent accessible voids in 3, and no satisfactory treatment could be appropriately done for the highly disordered water molecules (abnormal distorted thermal ellipsoids such as O5 and O7) in 5. Crystallographic data for 1-6 are summarized in Table 1. CCDC: 1012518-1012523 for 1-6 contains the supplementary crystallographic data, which are available free of charge from The Cambridge Crystallographic Data Centre via www.ccdc.cam.ac.uk/data_request/cif.

Results and discussion

Syntheses and characterization



Scheme 2 Schematic representation of self-assembly processes for complexes 1-6

All the complexes were synthesized by the self-assembly of [Mn^{III}(Schiff-base)]⁺ cations and [Fe^{III}(L)(CN)₃]⁻ anions (L = mpzcq, qcq), as illustrated in scheme 2. The precursors of [Mn^{III}(Schiff-base)(H₂O)]ClO₄ and PPh₄[Fe^{III}(L)(CN)₃]·H₂O are insoluble in water, but they are soluble in organic solvents such as the methanol and acetonitrile. In contrast, the precursor of K[Fe^{III}(L)(CN)₃]·H₂O is insoluble in organic solvents but could be well dissolved in aqueous solution. The different solvent

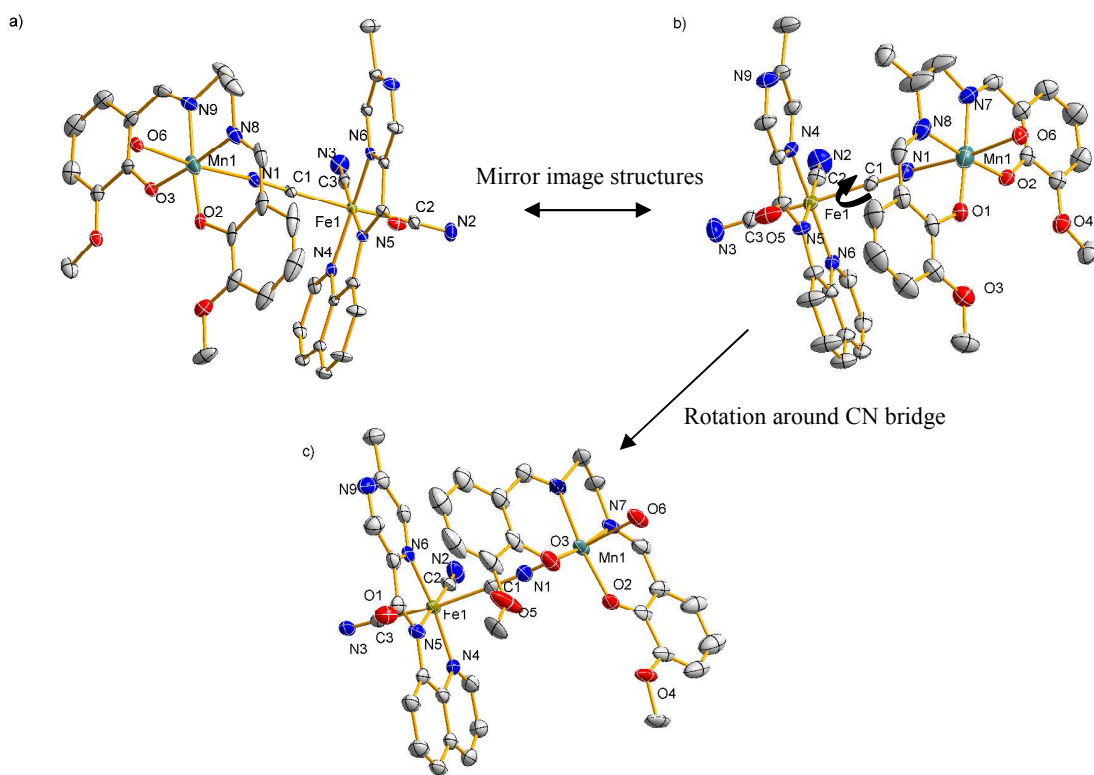


Fig. 1 ORTEP (30%) drawing of molecular units for **1** (a), **2** (b) and **3**(c) with selected atom-labeling schemes. (Hydrogen atoms and crystallized solvent molecules are omitted for clarity)

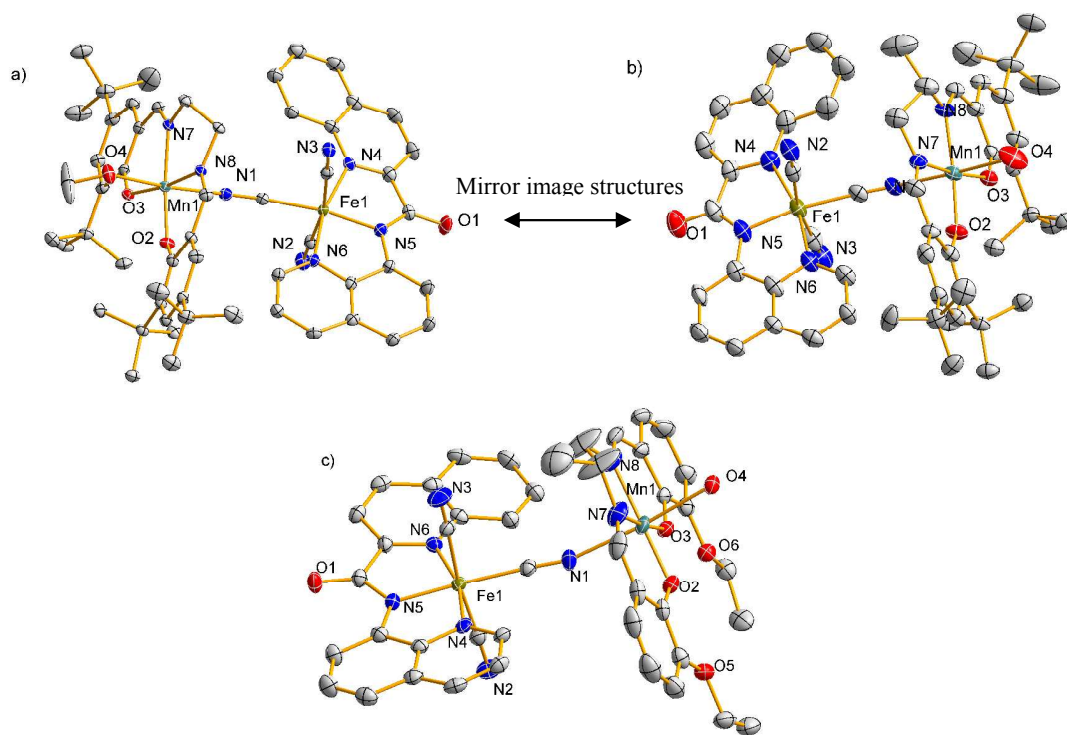


Fig. 2 ORTEP (30%) drawing of molecular units for **4** (a), **5** (b) and **6**(c) with selected atom-labeling schemes. (Hydrogen atoms and crystallized solvent molecules are omitted for clarity)

preferences of these reaction precursors facilitate us to tune the solvent polarity and the ratio of the mixed solvents so that the reaction process could be affected. Nevertheless, it is still insufficient to just change the reaction solvents, auxiliary reagents need to be introduced into the reaction systems to affect the self-assembly process. In this work, the triethylamine or lanthanide metal nitrate salts were added into the reaction mixtures because we firstly intended to construct new type of 3d-4f magnetic systems. Unfortunately, these additives failed to produce the expected complexes but do exert an influence on the structures of final products. Obviously, the structures of the formed complexes are simple function of neither the reaction precursors nor solvents nor auxiliary reagents but together these reaction variables induce the subtle change of the final structures. IR spectra of **1-6** all display absorption peaks at around 2120 cm^{-1} , which are characteristic absorption bands expected for cyanide groups.⁶³ The absorption bands at $1620\text{-}1630\text{ cm}^{-1}$ and $1400\text{-}1600\text{ cm}^{-1}$ could be assigned to stretching vibrations of N=C and benzene ring on the ligands of Schiff bases and/or the qq/mpzq.

Crystal structures

The selected bond lengths and angles of complexes **1-6** are listed in Table 2. The molecular asymmetric units of these complexes are shown in Fig. 1 and Fig. 2. The extended structures of these complexes are all depicted in Fig. S1-S4 in the Electronic Supplementary Information (ESI).

Complexes **1-6** are all cyano-bridged dinuclear $\text{Mn}^{\text{III}}\text{-NC-Fe}^{\text{III}}$ structures, which are also comparable to the previously reported complexes derived from other Mn^{III} (Schiff base) and tricyanidoferrate building blocks.^{45,53,55,56} However, these complexes show a gradual change in molecular geometries such as the rotation of the subunits, the coordination mode of tricyanidoferrate building blocks and the bond lengths and angles. Indeed, these molecular geometries have their influence on magnetic orbital overlapping and then affect the magnetic exchanges mechanism of $\text{Mn}^{\text{III}}\text{-NC-Fe}^{\text{III}}$ systems.³⁴ All the six complexes crystallize in the space groups of $P\ 2_1/n$ except for **3**, which has the space group of $P-1$. In their molecular units as shown in Fig. 1 and Fig. 2, the Mn^{III} (Schiff base) cations are axially coordinated by *mer*- $[\text{Fe}^{\text{III}}(\text{L})(\text{CN})_3]^-$ anions via a single cyanide (CN) bridge, leading to the formation of dinuclear $\text{Mn}^{\text{III}}\text{-NC-Fe}^{\text{III}}$ entities. For the moiety of Mn^{III} (Schiff base) cations, salen/salpn adopts a quasi-planar chelate mode³⁵ to coordinate to center Mn^{III} ion defining the equatorial plane, leaving one axial position occupied by N atom from cyanide group of *mer*- $[\text{Fe}^{\text{III}}(\text{L})(\text{CN})_3]^-$ and the other site capped by water or methanol molecules. The coordination environment of Mn^{III} center could be described as a typical elongated octahedron because the axial Mn-N/O bond lengths [$2.242(4)\text{-}2.340(7)\text{ \AA}$] are significantly longer than the equatorial Mn-N/O distances [$1.854(5)\text{-}1.992(5)\text{ \AA}$], revealing the characteristic Jahn-Teller effect of Mn^{III} ions. The Mn-N-C angles of the cyanide bridges in these complexes deviate significantly from linearity with values ranging from $149.0(2)$ to $165.2(4)^\circ$.

For the $[\text{Fe}^{\text{III}}(\text{L})(\text{CN})_3]^-$ unit, one cyanide group acts as bridge ligand with other two terminal. The Fe center also adopts distorted octahedral coordination environment (three C atoms from cyanide groups and three N atoms from L) with the Fe-C

and Fe-N bond length ranges of $1.928(9)\text{-}1.979(5)\text{ \AA}$ and $1.872(5)\text{-}2.027(4)\text{ \AA}$, respectively. In all these complexes, the bond distances of Fe-N_{amide} ($1.872(5)\text{-}1.890(7)\text{ \AA}$) are shorter than those of Fe-N_{aromatic rings} ($1.960(4)\text{-}2.027(4)\text{ \AA}$), which reveals the σ -donor effect of the deprotonated amide for $[\text{Fe}^{\text{III}}(\text{L})(\text{CN})_3]^-$ unit.⁵⁶ As expected, the Fe-C \equiv N angles of these complexes are within a narrow range from $175.3(4)$ to $179.2(9)^\circ$, indicating the three atoms are in good linear configuration.

From the above descriptions, complexes **1-6** do show quite similar subunits of Mn^{III} (Schiff base) and the $[\text{Fe}^{\text{III}}(\text{L})(\text{CN})_3]^-$ though the functional groups on salen-type ligands or L are different. However, the self-assembly of such two structural subunits could produce always variable molecular geometries that are dependent on the steric effect, electron effect as well as the reaction conditions. As shown in Fig. 1 and Fig. 2, the asymmetric unit of $\text{Mn}^{\text{III}}\text{-NC-Fe}^{\text{III}}$ dinuclear molecules of **1** and **4** are nearly the mirror image structures of **2** and **5**, respectively. Interestingly, the structural subunits of Mn^{III} (Schiff base) and $[\text{Fe}^{\text{III}}(\text{L})(\text{CN})_3]^-$ could undergo rotation around the cyanide bridges and lead to the formation of complex **3**. Because of this type of structural rotation, the molecular geometrical parameters of **3** are significantly different from **1** and **2**. For example, the dihedral angles of plane 1 (created through atoms of Fe1, C1, C2 and C3) and plane 2 (created through atoms of Mn1, N1, O6 and C30) in complexes **1** and **2** are in the narrow range from $12.5\text{-}14.9^\circ$, while the value for **3** is 60.1° . Besides, the critical Mn1-N1-C1 angles of the cyanide bridge (164.1°) as well as the torsion angle of Mn1-N1-C1-Fe1 (113.6°) in complex **3** are also quite different from those found for **1** (159.3° , 27.1°) and **2** (157.0° , 31.1°). The somewhat longer Fe-C1/C3 distances for **3** ($1.979(5)$, $1.972(5)\text{ \AA}$) could be also ascribed to such structural rotation which produce additional steric effect. Notably, there are two types of local arrangements for Mn^{III} (Schiff base) and $[\text{Fe}^{\text{III}}(\text{L})(\text{CN})_3]^-$ involved in the molecular units of **1-6**. For **1-3**, the molecular plane of $[\text{Fe}^{\text{III}}(\text{L})(\text{CN})_3]^-$ (created through atoms of N4, N5, N6) is approximately parallel to the equatorial plane of Mn^{III} (Schiff base) (dihedral angles: $15.9\text{-}22.0^\circ$) with the two terminal cyanide groups presented in *cis*-mode. In contrast, the two planes in **4-6** are found to be nearly perpendicular to each other (dihedral angles: $67.2\text{-}70.7^\circ$) and the two terminal cyanide groups are arranged in *trans*-mode. To our knowledge, the second type coordination mode shown by **4-6** is quite rare for the dinuclear complexes derived from Mn^{III} (Schiff base) and *mer*-tricyanidoferrate building blocks.^{45,53,55,56}

For the intermolecular contacts, the $3\text{-CH}_3\text{O}$ or $3\text{-CH}_2\text{CH}_2\text{O}$ groups on salen-type ligands in complexes **1-3** and **6** induce the formation of supramolecular $\text{FeMn}\dots\text{MnFe}$ dimers via hydrogen bond interactions, as shown in Fig. S1. Then, the formed Fe_2Mn_2 dimers further weakly contact with each other via the $\pi\text{-}\pi$ stacking between adjacent aromatic ring on $[\text{Fe}^{\text{III}}(\text{L})(\text{CN})_3]^-$, finally leading to the 1-D supramolecular chain structures (Fig. S2). It is worth noting that the formed supramolecular $\text{Mn}^{\text{III}}\text{Fe}^{\text{III}}$ chains stack parallel to each other in **1-3** while they arrange as intersect fashions in **6**, as shown in Fig. S3. For complexes **4** and **5**, the extended structures (Fig. S4) are quite different from **1-3** and **6**. Because the *t*-Bu groups on salen-type ligands could not be efficiently involved in hydrogen bonding interactions, the $\text{MnFe}\dots\text{FeMn}$ dimers generated by $\pi\text{-}\pi$ interactions (Fig. S1) are

actually well isolated from each other. Interestingly, complexes **4** and **5** show typical channels along *c* axis which accommodate guest solvent molecules.

Magnetic properties

Temperature dependence of the direct-current (dc) magnetic susceptibility data of **1-6** were collected at 2 kOe in the temperature range of 1.8-300 K, as shown in Fig. 3.

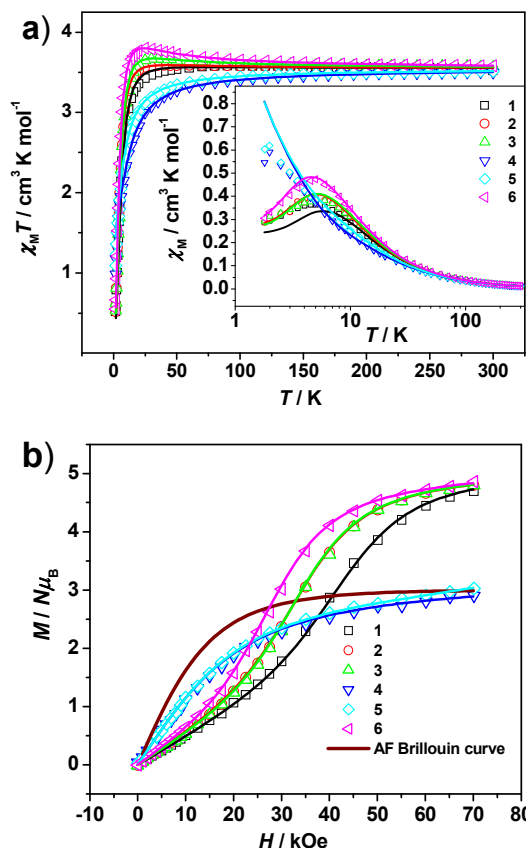
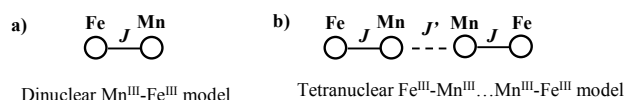


Fig. 3 (a) Temperature dependence of $\chi_M T$ and χ_M for **1-6** measured at 2 kOe; (b) Field dependence of the magnetization for **1-6** measured at 1.8 K (The solid lines represent the best simulations to the models described in the text; The line marked with AF Brillouin curve represents the antiferromagnetic coupled dinuclear $\text{Mn}^{\text{III}}\text{Fe}^{\text{III}}$)

At 300 K, the $\chi_M T$ values of **1-6** per $\text{Mn}^{\text{III}}\text{Fe}^{\text{III}}$ were all determined to be in the narrow region of 3.5-3.6 $\text{cm}^3 \text{K mol}^{-1}$ (Fig. 3a), which correspond to the spin-only value of 3.4 $\text{cm}^3 \text{K mol}^{-1}$ expected for a magnetically diluted spin system (one $S_{\text{Fe}} = 1/2$, one $S_{\text{Mn}} = 2$) assuming $g = 2$. Upon cooling, the $\chi_M T$ values of the **1** and **2** remain almost constant in the high temperature region but show a dramatic decrease in the low temperature region until reaching 0.5 $\text{cm}^3 \text{K mol}^{-1}$ at 1.8 K. For **3** and **6**, they undergo a gradual increase as the temperature is lowered and reach the maximum values of 3.7-3.8 $\text{cm}^3 \text{K mol}^{-1}$ at around 30 K. Below this temperature, a downturn of $\chi_M T$ values to 0.5-0.6 $\text{cm}^3 \text{K mol}^{-1}$ at 1.8 K occurs. Different from **3** and **6**, complexes **4** and **5** show quite different magnetic thermal behaviors in which the $\chi_M T$ values continuously decrease upon cooling until reach the minimum value of 1.0 $\text{cm}^3 \text{K mol}^{-1}$ at 1.8 K. The χ_M vs T curves of **1-6** are also plotted, as shown in the inset of Fig. 3a. For **1-3** and **6**, obvious peaks are detected at about 5 K, while they are

nearly invisible for **4** and **5**. The field-dependent magnetizations of **1-6** were measured at 1.8 K, as shown in Fig. 3b. The magnetizations of **1-3** and **6** increase with the increase of the dc field and reach 4.7-4.8 $N\mu_B$ at 70 kOe. However, The $M-H$ curves show typical field dependence “S” shape and the high field values are significantly higher than the theoretical values of 3.0 $N\mu_B$ expected for antiferromagnetic coupled dinuclear $\text{Fe}^{\text{III}}\text{Mn}^{\text{III}}$ units. In contrast, the magnetizations of **4** and **5** continuously increase with the increase of the dc field but no “S” shape of $M-H$ curves were detected. Besides, the saturated values of **4** and **5** (2.5-3 $N\mu_B$) are pretty smaller than those of **1-3** and **6**, but match to the Brillouin curve for antiferromagnetic coupled dinuclear $\text{Mn}^{\text{III}}\text{Fe}^{\text{III}}$ system, indicating the magnetic exchanges mechanism of **4** and **5** might be different from **1-3** and **6**.



Scheme 4 The magnetic model used for complexes **1-6**

Table 3 The magnetic fit parameters for complexes **1-6**

Complexes	Fitting parameters			
	J/cm^{-1}	J'/cm^{-1}	D/cm^{-1}	g
1	3.2	-0.65	-1.8	2.0
2	2.8	-0.5	-1.9	2.0
3	3.7	-0.5	-2.0	2.0
4	-3.0	-	-2.1	2.0
5	-2.1	-	-1.8	2.0
6	4.2	-0.4	-1.9	2.0

To probe the magnetic coupling constants of these systems, a simple dinuclear $\text{Mn}^{\text{III}}\text{-Fe}^{\text{III}}$ model (Scheme 4a) was used to describe their magnetism. Based on spin Hamiltonian: $H = -2J(S_{\text{Mn}} \cdot S_{\text{Fe}}) + D_{\text{Mn}} S_{z, \text{Mn}}^2$ (J represents the intramolecular $\text{Mn}^{\text{III}} \dots \text{Fe}^{\text{III}}$ interactions, D_{Mn} represents the zero field split effect of Mn^{III} ions), the data of **1-6** in the whole temperature region was simulated using Magpack program. Unfortunately, only **4** and **5** gave the acceptable parameters, which are listed in Table 3. The susceptibility and magnetization data of **1-3** and **6** in particular for the data in low temperature region were poorly simulated without satisfactory match of the experimental data and the simulated ones. From the crystal structures, the supramolecular $\text{FeMn} \dots \text{MnFe}$ dimers are generated via hydrogen bond interactions. Therefore, the $\text{Mn}^{\text{III}} \dots \text{Mn}^{\text{III}}$ interactions could not be safely neglected and complexes **1-3** and **6** should be considered as tetranuclear entities, $\text{Fe}^{\text{III}}\text{-Mn}^{\text{III}} \dots \text{Mn}^{\text{III}}\text{-Fe}^{\text{III}}$, in which the magnetic couplings of $\text{Mn}^{\text{III}} \dots \text{Fe}^{\text{III}}$ and $\text{Mn}^{\text{III}} \dots \text{Mn}^{\text{III}}$ pathways are defined as J and J' , respectively (Scheme 4b). Based on the spin Hamiltonian: $H = -2J(S_{\text{Mn1}} \cdot S_{\text{Fe1}} + S_{\text{Mn1}} \cdot S_{\text{Fe2}}) - 2J'S_{\text{Mn1}} \cdot S_{\text{Mn2}} + D_{\text{Mn}}(S_{z, \text{Mn1}}^2 + S_{z, \text{Mn2}}^2)$, Magpack program was again employed to simulate the data, and the best match in the whole temperature range gave the parameters which are listed in Table 3. The obtained parameters are reasonable for $\text{Fe}^{\text{III}}\text{-CN-Mn}^{\text{III}}$ systems and also comparable to those values reported for analogous complexes. Notably, the S-shaped $M-H$ curves of **1-3** and **6** could be well reproduced by the simulation data based on

the set of obtained parameters, further indicating the importance of the $\text{Mn}^{\text{III}} \dots \text{Mn}^{\text{III}}$ interactions for the final magnetic properties.

Discussions

It is well known the $\text{Fe}^{\text{III}}\text{-CN-Mn}^{\text{III}}$ systems could be either ferro- or antiferromagnetically coupled.^{34,40} Unfortunately, very clear magneto-structural correlation in this type of systems that include all the reported results are not available so far, indicating the magnetic interactions are not a simple function of any single structural parameter but together these variables that determine the interactions to be antiferromagnetic or ferromagnetic. However, the magneto-structural correlation for the six dinuclear $\text{Fe}^{\text{III}}\text{-CN-Mn}^{\text{III}}$ complexes of **1-6** in this work seems to be possible to be clarified considering their structures and magnetic properties. From the structural point of view, there are several critical factors that are most important to the final magnetic behaviors: (1) the molecular orbital describing the unpaired electron in low-spin Fe^{III} center (electronic configuration $t_{2g}^5 e_g^0$); (2) the angle of $\text{Mn-N-C}_{\text{cyanide}}$ (θ) involving the cyanide group that connects the Mn^{III} and Fe^{III} centers; (3) the intermolecular short contacts that mediated via hydrogen bonds or $\pi\text{-}\pi$ interactions. For the magnetic orbital of low-spin Fe^{III} center, it is highly dependent on the local coordination environment. From previous relevant studies,³⁴ the magnetic orbital of *mer*- $[\text{Fe}^{\text{III}}(\text{L})(\text{CN})_3]^-$ corresponds to d_{xz} type (z axis is defined as the bridging cyanide direction), whose orthogonality with the d_z^2 orbital on Mn^{III} centers can be lost as the bending of the $\text{Mn-N-C}_{\text{cyanide}}$ increases, leading to magnetic coupling type from ferro- to antiferromagnetic. The angles of $\text{Mn-N-C}_{\text{cyanide}}$ in **1-6** are given in Fig. 4 together with the corresponding coupling constants obtained from the magnetic analysis. From the diagram, it is indeed revealed that the coupling constants for **1-6** are highly dependent on the $\text{Mn-N-C}_{\text{cyanide}}$ angles, in which bent Mn-N-C-Fe linkages prefer to antiferromagnetic coupling while more linear ones are in favor of ferromagnetic nature. It is worth noting that such a $\text{Mn-N-C}_{\text{cyanide}}$ angle dependent rule is also suitable for other $\text{Fe}^{\text{III}}\text{-CN-Mn}^{\text{III}}$ complexes reported in the literatures⁴⁰.

Another important factor, as motioned above, would be the intermolecular short contacts involved in the systems. The X-ray crystal diffraction reveals that the $\text{Fe}^{\text{III}}\text{-CN-Mn}^{\text{III}}$ dinuclear units in **1-3** and **6** are strongly dimerized via hydrogen bond interactions between two neighboring Mn^{III} ions while those are insignificant in **4** and **5**. Consequently, the magnetic behaviors shown by **1-3** and **6** are actually contributed by both the ferromagnetic $\text{Fe}^{\text{III}} \dots \text{Mn}^{\text{III}}$ couplings (J) and antiferromagnetic $\text{Mn}^{\text{III}} \dots \text{Mn}^{\text{III}}$ interactions (J'). To gain insight into such mechanism, we performed the theoretical simulations of $M\text{-}H$ curves of supramolecular $\text{FeMn} \dots \text{MnFe}$ dimers using continuous changing set of parameters, as shown in Fig. 5. From the theoretical curves, the S-shape of the $M\text{-}H$ curves is highly dependent on the weak antiferromagnetic $\text{Mn}^{\text{III}} \dots \text{Mn}^{\text{III}}$ interactions (J') but independent on the ferromagnetic $\text{Fe}^{\text{III}} \dots \text{Mn}^{\text{III}}$ couplings (J), indicating that the field induced metamagnetic behaviors of **1-3** and **6** (S-shape $M\text{-}H$ curves) actually originated from the interdimer $\text{Mn}^{\text{III}} \dots \text{Mn}^{\text{III}}$ interactions. When such $\text{Mn}^{\text{III}} \dots \text{Mn}^{\text{III}}$ interactions are significantly weakened by replacing the 3- CH_3O or 3- $\text{CH}_3\text{CH}_2\text{O}$ with *t*-Bu groups, the S-shape feature of $M\text{-}H$ curves disappeared, as shown by complexes **4** and **5**.

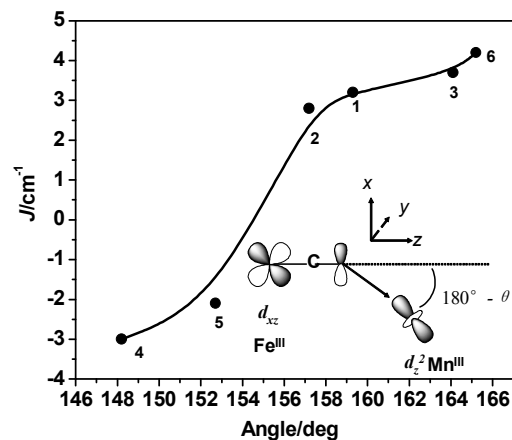


Fig. 4 The relationship of $\text{Mn-N-C}_{\text{cyanide}}$ angles and the coupling constants for **1-6**. (The solid black line is guide line)

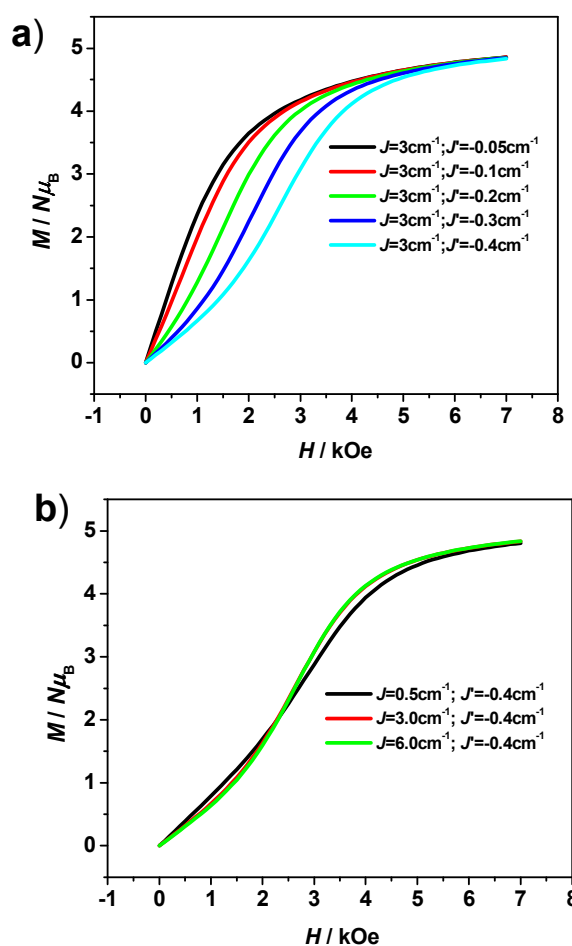


Fig. 5 The theoretical simulation of $M\text{-}H$ curves of supramolecular $\text{FeMn} \dots \text{MnFe}$ dimers with continuous changing set of parameters

It is worth noting that the models devised for analyzing the magnetic properties of **1-6** are still somewhat rough because some other weak contacts such as the $\pi\text{-}\pi$ interactions are not taken into account. But considering that the spin values of Fe^{III} ions involved in the weak $\pi\text{-}\pi$ stacking are actually very small and the $\text{Fe} \dots \text{Fe}$ distances are very large (larger than 8.7 Å), the

magnetic contributions from π - π interactions could be safely neglected in these complicated magnetic systems.

Conclusions

In summary, six new cyano-bridged dinuclear $\text{Mn}^{\text{III}}\text{-NC-Fe}^{\text{III}}$ complexes (**1-6**) derived from Mn^{III} (Schiff base) and *mer*- $[\text{Fe}^{\text{III}}(\text{L})(\text{CN})_3]$ have been synthesized, structurally characterized and magnetically studied. Notably, these complexes show subtle changes in molecular geometric parameters and structures, which are proved to be important for their final magnetic properties. From the analysis of magneto-structural correlation, it is found that the intramolecular coupling nature of $\text{Fe}^{\text{III}}\text{-CN-Mn}^{\text{III}}$ is dependent on the overlap of magnetic orbitals of Fe^{III} and Mn^{III} , which are revealed to be highly relevant to the $\text{Mn-N-C}_{\text{cyanide}}$ angles. Moreover, the mechanism of the field induced metamagnetic behaviors of these complexes was clarified from the point of structures by comparing the experimental data with the theoretical simulations. The next important work is to investigate how to optimize these geometric parameters to enhance the coupling interactions as well as the magnetic anisotropy, the related work is under way in our group

Acknowledgements

The authors are grateful for financial support from the National Natural Science Foundation of China (Nos. 1601310042 and 51072071), Doctoral Innovation Program Foundation of China (No. 1721310119) and the Startup Foundation for Advanced Talents of Jiangsu University (No. 11JDG106).

Notes and references

a School of Chemistry and Chemical Engineering, Jiangsu University, Zhenjiang 212013, China. Fax: +86-511-8879180; Tel: +86-511-88791800; E-mail: xiaopingshen@163.com.
b School of Biology and Chemical Engineering, Jiangsu University of Science and Technology, Zhenjiang 212003, China

- O. M. Yaghi, G. Li and H. Li, *Nature*, 1995, **378**, 703.
- L. M. C. Beltran and J. R. Long, *Acc. Chem. Rev.*, 2005, **38**, 325.
- N. Roch, S. Florens, V. Bouchiat, W. Wernsdorfer and F. Balestro, *Nature*, 2008, **453**, 633.
- J. Lee, O. K. Farha, J. Roberts, K. A. Scheidt, S. T. Nguyen and J. T. Hupp, *Chem. Soc. Rev.*, 2009, **38**, 1450.
- H. L. Sun, Z. M. Wang and S. Gao, *Coord. Chem. Rev.*, 2010, **254**, 1081.
- F. Troiani and M. Affronte, *Chem. Soc. Rev.*, 2011, **40**, 3119.
- J. M. Clemente-Juan, E. Coronado and A. Gaita-Ariño, *Chem. Soc. Rev.*, 2012, **41**, 7464.
- S. D. Jiang, B. W. Wang, H. L. Sun, Z. M. Wang and S. Gao, *J. Am. Chem. Soc.*, 2011, **133**, 4730.
- Y. L. Wang, Y. Ma, X. Yang, J. K. Tang, P. Cheng, Q. L. Wang, L. C. Li and D. Z. Liao, *Inorg. Chem.*, 2013, **52**, 7380.
- E. Colacio, J. Ruiz, E. Ruiz, E. Cremades, J. Krzystek, S. Carretta, J. Cano, T. Guidi, W. Wernsdorfer and E. K. Brechin, *Angew. Chem., Int. Ed.*, 2013, **52**, 9130.
- M. Verdagner, *Science*, 1996, **272**, 698.
- S. M. Holmes and G. S. Girolami, *J. Am. Chem. Soc.*, 1999, **121**, 5593.
- E. Dujardin, S. Ferlay, X. Phan, C. Desplanches, C. Cartier dit Moulin, P. Sainctavit, F. Baudelet, F. Dartyge, P. Veillet and M. Verdagner, *J. Am. Chem. Soc.*, 1998, **120**, 11347.
- Z. H. Ni, H. Z. Kou, L. F. Zhang, C. Ge, A. L. Cui, R. J. Wang, Y. Li and O. Sato, *Angew. Chem., Int. Ed.*, 2005, **44**, 7742.
- C. G. Freiherr von Richthofen, A. Stammler, H. Bogge, M. W. DeGroot, J. R. Long and T. Glaser, *Inorg. Chem.*, 2009, **48**, 10165.
- F. Pan, Z. M. Wang and S. Gao, *Inorg. Chem.*, 2007, **46**, 10221.
- S. Nastase, C. Maxim, M. Andruh, J. Cano, C. Ruiz-Perez, J. Faus, F. Lloret and M. Julve, *Dalton Trans.*, 2011, **40**, 4898.
- M. X. Yao, Q. Zheng, X. M. Cai, Y. Z. Li, Y. Song and J. L. Zuo, *Inorg. Chem.*, 2012, **51**, 2140.
- I. Y. Yoo, D. W. Ryu, J. H. Yoon, A. R. Sohn, K. S. Lim, B. K. Cho, E. K. Koh and C. S. Hong, *Dalton Trans.*, 2012, **41**, 1776.
- H. Z. Kou, Z. H. Ni, C. M. Liu, D. Q. Zhang and A. L. Cui, *New J. Chem.*, 2009, **33**, 2296.
- I. Boldog, F. J. Munoz-Lara, A. B. Gaspar, M. C. Munoz, M. Sereidyuk and J. A. Real, *Inorg. Chem.*, 2009, **48**, 3710.
- T. Liu, Y. J. Zhang, S. Kanegawa and O. Sato, *Angew. Chem., Int. Ed.*, 2010, **49**, 8645.
- M. X. Yao, Z. Y. Wei, Z. G. Gu, Q. Zheng, Y. Xu and J. L. Zuo, *Inorg. Chem.*, 2011, **50**, 8636.
- Y. Z. Zhang, U. P. Mallik, R. Clerac, N. P. Rath and S. M. Holmes, *Chem. Commun.*, 2011, **47**, 7194.
- R. Lescouezec, J. Vaissermann, F. Lloret, M. Julve and M. Verdagner, *Inorg. Chem.*, 2002, **41**, 5943.
- J. Kim, S. Han, K. I. Pokhodnya, J. M. Migliori and J. S. Miller, *Inorg. Chem.*, 2005, **44**, 6983.
- D. Li, S. Parkin, R. Clerac and S. M. Holmes, *Inorg. Chem.*, 2006, **45**, 7569.
- Z. G. Gu, Q. F. Yang, W. Liu, Y. Song, Y. Z. Li, J. L. Zuo and X. Z. You, *Inorg. Chem.*, 2006, **45**, 8895.
- M. Shatruk, A. Dragulescu-Andrasi, K. E. Chambers, S. A. Stoian, E. L. Bominaar, C. Achim and K. R. Dunbar, *J. Am. Chem. Soc.*, 2007, **129**, 6104.
- Y. Z. Zhang, S. Gao, Z. M. Wang, G. Su, H. L. Sun and F. Pan, *Inorg. Chem.*, 2005, **44**, 4534.
- Z. H. Ni, J. Tao, W. Wernsdorfer, A. L. Cui and H. Z. Kou, *Dalton Trans.*, 2009, 2788.
- D. P. Zhang, L. F. Zhang, X. Chen and Z. H. Ni, *Trans. Met. Chem.*, 2011, **36**, 539.
- D. Visinescu, L. M. Toma, J. Cano, O. Fabelo, C. Ruiz-Perez, A. Labrador, F. Lloret and M. Julve, *Dalton Trans.*, 2010, **39**, 5028.
- H. Miyasaka, A. Saitoh and S. Abec, *Coord. Chem. Rev.*, 2007, **251**, 2622.
- H. B. Zhou, J. Wang, H. S. Wang, Y. L. Xu, X. J. Song, Y. Song and X. Z. You, *Inorg. Chem.*, 2011, **50**, 6868.
- X. P. Shen, H. B. Zhou, Q. Zhang, Y. Xu and H. Zhou, *Eur. J. Inorg. Chem.*, 2012, 5050.
- X. P. Shen, Q. Zhang, H. B. Zhou, H. Zhou and A. H. Yuan, *New J. Chem.*, 2012, **36**, 1180.
- H. B. Zhou, Q. Zhang, Y. Q. Yang, Y. Xu, H. Zhou and X. P. Shen, *Inorg. Chim. Acta*, 2013, **402**, 97.
- X. P. Shen, H. B. Zhou, J. H. Yan, Y. F. Li and H. Zhou, *Inorg. Chem.*, 2014, **53**, 116.
- Y. Y. Wang, H. B. Zhou, X. P. Shen and A. H. Yuan, *Inorg. Chim. Acta*, 2014, **414**, 53.
- Q. Zhang, H. B. Zhou, X. P. Shen, H. Zhou and Y. Q. Yang, *New J. Chem.*, 2013, **37**, 941.
- H. B. Zhou, J. H. Yan, X. P. Shen, H. Zhou and A. H. Yuan, *Rsc. Adv.*, 2014, **4**, 61.
- J. Y. Yang, M. P. Shores, J. J. Sokol and J. R. Long, *Inorg. Chem.*, 2003, **42**, 1403.
- H. Y. Kwak, D. W. Ryu, J. W. Lee, J. H. Yoon, H. C. Kim, E. K. Koh, J. Krinsky and C. S. Hong, *Inorg. Chem.*, 2010, **49**, 4632.
- W. Liu, C. F. Wang, Y. Z. Li, J. L. Zuo and X. Z. You, *Inorg. Chem.*, 2006, **45**, 10058.
- H. R. Wen, C. F. Wang, Y. Song, S. Gao, J. L. Zuo and X. Z. You, *Inorg. Chem.*, 2006, **45**, 8942.
- X. M. Li, C. F. Wang, Y. Ji, L. C. Kang, X. H. Zhou, J. L. Zuo and X. Z. You, *Inorg. Chem.*, 2009, **48**, 9166.
- Y. J. Zhang, T. Liu, S. Kanegawa and O. Sato, *J. Am. Chem. Soc.*, 2010, **132**, 912.
- L. C. Kang, X. Chen, H. S. Wang, Y. Z. Li, Y. Song, J. L. Zuo and X. Z. You, *Inorg. Chem.*, 2010, **49**, 9275.
- R. Lescouezec, J. Vaissermann, L. M. Toma, R. Carrasco, F. Lloret and M. Julve, *Inorg. Chem.*, 2004, **43**, 2234.

- 52 H. R. Wen, Y. Z. Tang, C. M. Liu, J. L. Chen and C. L. Yu, *Inorg. Chem.*, 2009, **48**, 10177.
- 53 T. Senapati, C. Pichon, R. Ababei, C. Mathoniere and R. Clerac, *Inorg. Chem.*, 2012, **51**, 3796.
- 54 J. I. Kim, H. S. Yoo, E. K. Koh, H. C. Kim and C. S. Hong, *Inorg. Chem.*, 2007, **46**, 8481.
- 55 J. I. Kim, H. S. Yoo, E. K. Koh and C. S. Hong, *Inorg. Chem.*, 2007, **46**, 10461.
- 56 J. L. Kim, H. Y. Kwak, J. H. Yoon, D. W. Ryu, I. Y. Yoo, N. Yang, B. K. Cho, J. G. Park, H. Lee and C. S. Hong, *Inorg. Chem.*, 2009, **48**, 2956.
- 57 D. Zhang, H. Wang, L. Tian, H. Z. Kou, J. Jiang and Z. H. Ni, *Cryst. Growth Des.*, 2009, **9**, 3989.
- 58 H. Miyasaka, H. I. N. Matsumoto, N. Re, R. Crescenzi and C. Floriani, *Inorg. Chem.*, 1998, **37**, 255.
- 59 B. J. Kennedy and K. S. Murray, *Inorg. Chem.*, 1985, **24**, 1552.
- 60 O. Kahn, *Molecular Magnetism*, VCH Publishers, New York, 1993.
- 61 Bruker, *SMART, SAINT and XPREP: Area Detector Control and Data Integration and Reduction Software*, Bruker Analytical X-ray Instruments Inc.; Madison, Wisconsin, USA, 1995.
- 62 G. M. Sheldrick, *SHELXL-97, Program for the Refinement of Crystal Structure*, University of Göttingen, Germany, 1997.
- 63 K. Nakamoto, *Infrared and Raman Spectra of Inorganic and Coordination Compounds*, 5th ed.; Wiley: New York, 1997; Part B, pp105.
- 64 J. J. Borrás-Almenar, J. M. Clemente-Juan, E. Coronado and B. Tsukerblat, *Inorg. Chem.*, 1999, **38**, 6081.
- 65 J. J. Borrás-Almenar, J. M. Clemente-Juan, E. Coronado and B. Tsukerblat, *MAGPACK, Magnetic Properties Analysis Package for Spin Clusters*, version 00.1, 2000.
- 66 J. J. Borrás-Almenar, J. M. Clemente-Juan, E. Coronado and B. Tsukerblat, *J. Comput. Chem.*, 2001, **22**, 985.